On mechanisms of intense combustion noise emission

Thierry Schuller*, Nicolas Noiray, Daniel Durox and Sébastien Candel

Laboratoire EM2C, CNRS and Ecole Centrale Paris
92295 Châtenay-Malabry, France
thierry.schuller@em2c.ecp.fr

Abstract

Experiments were carried out to investigate mechanisms leading to strong noise production in unconfined combusting systems. The experimental set-up comprises a premixed laminar burner equipped with an actuation system used to modulate the flow at the burner lips around the mean operating conditions. Four different flame geometries, stabilization configurations and flow interactions were explored for premixed methane air flames in a mixture of constant equivalence ratio. Flame response to incoming flow modulations were analyzed by simultaneous measurements of velocity perturbations at the burner outlet, variations of the flame light emission and noise radiation. These signals were correlated using classical results of combustion noise theory. Phase locked images of the flame patterns were also acquired to examine the history of noise emission and locate the flame patterns corresponding to the instant of maximum noise production. Events corresponding to large and fast rates of variation of the flame surface area were identified as the main contribution to the overall radiated noise in all cases explored. This was verified hereby for a set of laminar flame flow interactions, which constitute elementary mechanisms occurring in turbulent combustion : a flame submitted to convective velocity waves, a flame interacting with vortices shed from the burner lips, mutual annihilations of neighboring flame elements and collective effects of an ensemble of small conical flames. These mechanisms investigated in unconfined configurations may also prevail in combustors operating at steady or slowly varying conditions, like those of gas turbines or jet engines, and may play an important role in acoustically coupled combustion instabilities.

INTRODUCTION

Suppression of combustion instabilities and reduction of sound emission from high performance combustors pose technical challenges which require an understanding of the mechanisms leading to noise production [1]. Among all noise sources, combustion contributions prevail for instance during engine warmup, partial load conditions or unstable operation [2].

The latter conditions may also lead to severe structural damages or early aging of the combustor envelope and should be avoided. While the main principles underlying the description of far-field noise radiated from a compact turbulent reacting region were outlined by Strahle in the middle seventies [3] and many later papers [4, 5, 6, 7, 8], the detailed mechanisms leading to intense noise production are less well documented [9, 10, 11].
This article aims to list some flame flow interactions at the origin of intense combustion noise emission. These mechanisms may be viewed as elementary interactions occurring in turbulent burners. The main result from combustion noise theory is a relation between the acoustic pressure p'_∞ radiated in the far-field of a compact flame and the net rate of change of the heat release rate in the reacting volume [6] :

$$p'_\infty(r,t) = \frac{\gamma-1}{4\pi r c^2}\int_V \frac{\partial \dot{Q}}{\partial t}(\mathbf{r}_0, t-\tau)dV(\mathbf{r}_0) \tag{1}$$

where $\dot{Q}$ is the volumetric heat release rate (J m^{-3} s^{-1}), r is the distance from the compact combustion zone to the observation point, τ the time required for the sound to cover the distance r and c the speed of sound. Compact and far-field conditions are fulfilled when $r \gg \lambda \gg L$, where λ is the sound wavelength and L is a characteristic flame length. Equation (1) takes a simple form for premixed flames in homogeneous mixture at a fixed equivalence ratio. The heat release rate $\dot{Q}$ can be expressed with the flame surface area A :

$$\int_V \dot{Q}dV = \int_A \rho Y_f S_d(-\Delta h_f^0)dA \tag{2}$$

where S_d is the flame speed. In the laminar case, S_d equals S_L the laminar burning velocity when stretch and curvature effects are ignored [12, 13]. The flame velocity S_L is a function of the equivalence ratio and injection conditions of the premixed reactants. In this expression, the integration is performed over the flame surface area $A(t)$, Y_f is the fuel mass fraction and Δh_f^0 (J kg^{-1}) the enthalpy released by conversion of a unit mass of fuel. For a premixed compact laminar flame at a fixed equivalence ratio one obtains :

$$p'_\infty(r,t) = \frac{\gamma-1}{4\pi r}\frac{\rho Y_f(-\Delta h_f^0)}{c^2} S_L \left[\frac{dA}{dt}\right]_{t-\tau} \tag{3}$$

This expression can also be rewritten in the following form [14, 15] :

$$p'_\infty(r,t) = \frac{\rho}{4\pi r}\left(E-1\right) S_L \left[\frac{dA}{dt}\right]_{t-\tau} \tag{4}$$

where $E = \rho_u/\rho_b$ is the volumetric expansion ratio of burned to unburned gases and ρ the air density at room temperature. It is also known from many experiments that the heat release rate is directly proportional to the light emission I of free radicals (CH^*, C_2^*, OH^*, ...) naturally present in the flame front. This relationship applies to premixed flame maintained at a fixed equivalence ratio and this use yields another elegant expression for the far-field pressure [16] :

$$p'_\infty(r,t) = N(r)\left[\frac{dI}{dt}\right]_{t-\tau} \tag{5}$$

This useful relation was checked in different experiments in the past [16, 17, 18, 19, 20] and more recently by our group for several flame geometries and flow interaction configurations [11, 21]. The coefficient N depends on the free radical observed, the equivalence ratio, the optical apparatus and the signal treatment chain. As radical light emission fluctuations I' and flame surface variations A' are proportional, the following relation was used to scale light emission signal in this study [21] :

$$\frac{A'}{\bar{A}} = \frac{I'}{\bar{I}} \tag{6}$$

where $\bar{I}$ and $\bar{A}$ are the mean light and flame surface quantities. From Eqs. (4) to (6), flame light emission I', flame surface A' and far-field acoustic pressure fluctuations p' are related by simple algebraic expressions. This is used below together with snapshots of the flame to investigate the detailed history of noise production during a set of flame flow interactions.

EXPERIMENTAL SETUP

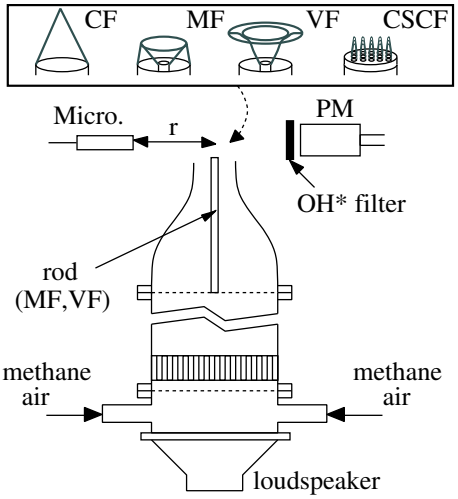

Figure 1: *Experimental setup.*

The experimental setup displayed in Fig. 1 comprises a burner with a $d = 22$mm nozzle exit diameter and a loud-speaker fixed at its base. The body of the burner is a cylindrical tube of 65 mm inner diameter containing a set of grids and a honeycomb grid followed by a convergent nozzle of contraction ratio $\sigma = 8.73$. It is designed to produce a steady laminar flow with a flat velocity profile at the burner exit for mean flow velocities up to 5 m s^{-1}. Using this apparatus, velocity disturbances at the burner outlet are reduced to low levels as $v_{rms}/\bar{v} < 0.01$ on the central axis for free jet injection conditions (without acoustic forcing). The burner is fed at its the bottom with a mixture of methane and air. Experiments presented hereby were carried out at fixed equivalence ratios. As internal flow disturbances are minimized, the influence of external flow modulations can be investigated. These perturbations

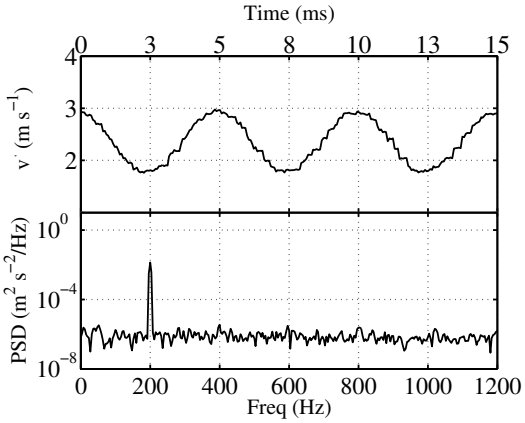

Figure 2: *Velocity time trace during harmonic modulation of the flow at the burner outlet and the corresponding PSD distribution.* MF *flame (Fig. 3),* $\Phi = 1.11$*,* $\bar{v} = 2.3\ m\ s^{-1}$*,* $v_{rms} = 0.4\ m\ s^{-1}$*,* $f_e = 200\ Hz$*.*

were produced by the loudspeaker driven by an amplifier, which is fed by a signal synthesizer. Using this driving system, harmonic velocity modulations around the mean steady velocity like those presented in Fig. 2 were obtained at the burner lips. Velocities were measured by Laser Doppler Velocimetry (LDV) on the burner symmetry axis at $z = 1.3$ mm above the nozzle exit plane. The time trace velocity in Fig. 2 is a purely harmonic signal as shown by the distribution of the Power Spectral Density (PSD) presented in the lower part of this figure with a frequency peak at $f = 200$ Hz well above the background noise. For all flow conditions and driving frequencies explored, a minimum data rate collection of 15 kHz with 70% validation was ensured. Other records exhibit similar features to those presented in Fig. 2 with a strong peak at the driving frequency and a very low harmonic level. Incoming flow perturbations in the experiments presented below can be considered purely sinusoidal at the nozzle exit. For the range of flow velocities and the two equivalence ratios considered in what follows, flames are naturally anchored on the burner lips and take a conical shape (Fig. 3, CF Statio). The burner can also be equipped with a 2 mm diameter cylindrical rod placed inside the convergent unit and centered on the axis to modify flame anchoring points. The flame can be stabilized simultaneously on the central rod and on the external burner lips, and take an "M" like shape (Fig. 3, MF Statio), but it can also be attached only to the central rod and adopt a "V" shape (Fig. 3, VF Statio). Stabilization as an "M" flame or a "V" flame can be obtained for the same flow velocity and equivalence ratio depending on the ignition location point. Once a regime is set, it remains stable without external intervention. Finally, the central rod can be replaced by a perforated plate flush mounted at the top of the burner nozzle. This plate features 2 mm diameter regularly spaced holes to study collective effects of 25 small conical flames (Fig. 3, CSCF Statio). The camera line of sight crosses a row of holes to get a clear image. The flame dynamics corresponding to these four configurations (CF, MF, VF and CSCF) is examined under harmonic flow perturbations, by simultaneously recording

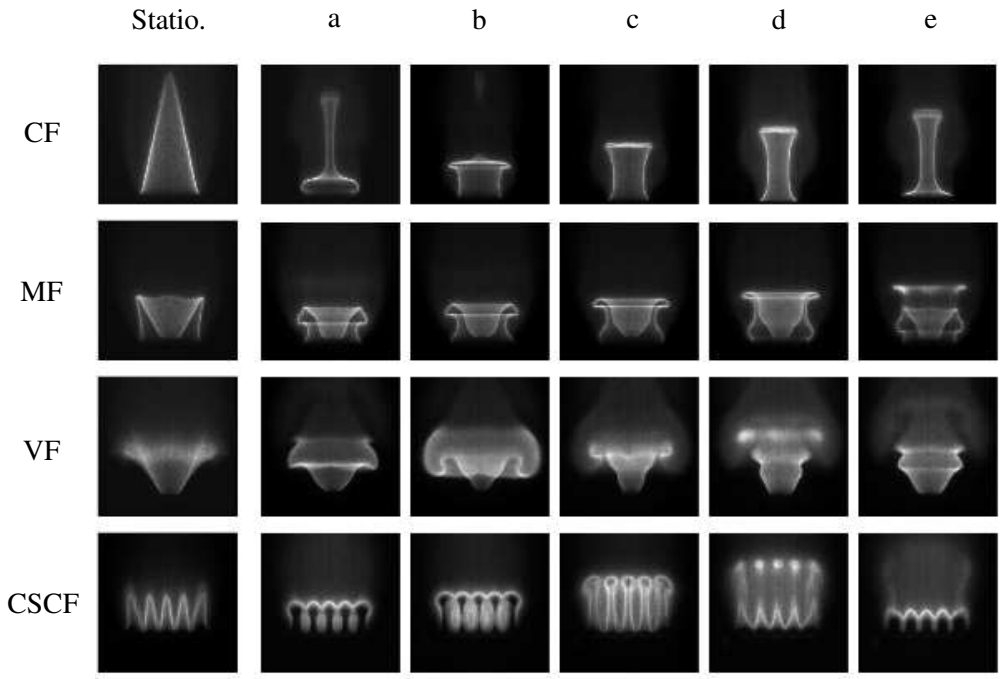

Figure 3: *Flames snapshots.* Statio. *: stationary shapes.* a-e *: cycle of excitation.* CF *: conical flame.* MF *: "M" shaped flame.* VF *: "V" shaped flame.* CSCF *: collection of small conical flames.*

the velocity modulation at the burner exit, fluctuations of the flame natural emission and the noise radiated in the laboratory. Axial velocity was measured by LDV at the burner outlet as explained previously. Evolution of the flame emission during flow modulation was analyzed with a photomultiplier (Fig. 1, PM) equipped with a 2 nm narrow band OH^* filter centered on $\lambda = 308$ nm. Noise emission was recorded using a B&K microphone (Fig. 1, Micro.) placed at a distance $r = 253$ mm away from the burner axis. In principle, this distance is too small to completely fulfill far-field conditions for noise emission from a compact flame submitted to external perturbations with frequencies of a hundred Hz as required by combustion noise theory [22], but it is adequate for the purpose of the paper. LDV, PM and Micro output voltages were simultaneously recorded and acquired on an A/D board piloted by a computer at an acquisition frequency $f_a = 16\,384$ Hz during a 2 seconds recording time. This acquisition duration enables to record at least 100 periods for the lowest driving frequency $f_e = 50$ Hz and 800 periods for the highest frequency $f_e = 400$ Hz. These informations are processed to extract retarded time rates of change of the flame light chemilunescence using Eq. (5). As flow interactions are laminar, records were reproducible from cycle to cycle. Sound pressure levels (SPL) were computed using the following definition : $\text{SPL(dB)} = 20 \log_{10} (p_{rms}/p_{ref})$ where $p_{ref} = 2.\,10^{-5}$ Pa is a reference acoustic pressure.

Velocity, flame emission and acoustic signals signals were recorded together with phase averaged images of the flame patterns at regularly spaced instants during the driving cycle using

Table 1: *Summary of operating conditions*

	Φ	f_e (Hz)	SPL (dB)	$\bar{S}$ (m^2)	$S_{\rm rms}$ (m^2)	$\bar{v}$ (m s^{-1})	$v_{\rm rms}$ (m s^{-1})
CF	1.11	50	70	$1.8\,10^{-3}$	$1.9\,10^{-4}$	1.7	0.8
MF	1.11	200	90	$2.1\,10^{-3}$	$4.0\,10^{-4}$	2.3	0.4
VF	1.11	100	94	$2.1\,10^{-3}$	$9.0\,10^{-4}$	2.3	0.6
CSCF	0.95	400	93	–	–	5.0	0.9

an intensified CCD camera (ICCD). Each image is formed by averaging 100 snapshots with an exposure time $\Delta t = 100$ μs (Fig. 3 CF, MF, VF, CSCF a-e). As configurations explored are laminar and the exposure time small enough compared to the driving period $T_e = 1/f_e$ ($T_e = 2.5$ to 20 ms), each phase averaged image can be considered as a snapshot of the flame pattern at a precise instant in the driving cycle. Cycle to cycle reproducibility can also be assessed by examining the image sharpness. Except some blurring effects on the flame periphery of the stationary "V" shape flame and neighboring inner reaction zones of the collection of small conical flames, other phase averaged images are perfectly sharp and one may easily follow the flame contour. For each driving frequency, 21 images at regularly spaced phases were taken to cover a complete excitation cycle and post-processed to extract the flame contour. Except for the collections of conical flames case CSCF, flame surface areas were computed assuming a cylindrical symmetry. Using Eqs. (4) and (6), relative fluctuation flame surface area over a cycle can be directly compared to relative flame light variations and noise radiation. Main operating conditions are summarized in Table 1. In the results presented below, the specific heat ratio was taken equal to $\gamma = 1.4$, the acoustic time propagation delay $\tau = r/c = 7.38\,10^{-4}$ s, where $r = 253$ mm is the burner axis to microphone distance and $c = 343$ m s^{-1} is the speed of sound at room temperature $T = 293$ K. The air density is taken equal to $\rho_\infty = 1.205$ kg m^{-3}. Flame speeds were taken from Ref. [23] $S_L = 0.38$ m s^{-1} for $\Phi = 1.11$ and $S_L = 0.34$ m s^{-1} for $\Phi = 0.95$. The volumetric expansion ratio $E = \rho_u/\rho_b = W_u T_b/W_b T_u = 7.4$ was estimated from the temperature ratio of burned to unburned gases around stoichiometry. Analysis of PM and acoustic pressure signals together with flame surface area A evolution extracted from the images is carried out in what follows.

RESULTS AND DISCUSSION

The first flow interaction is that of a conical flame submitted to convective waves (Fig. 3-CF, a-e). Under strong harmonic forcing $v_{rms}/\bar{v} = 0.47$, the shape of the flame exhibits periodic wrinkles with a large bulge convected from the burner lips to the flame tip inducing moderate flame surface variation $A_{rms}/\bar{A} = 0.11$. Nevertheless, the creation of this bulge leads to flame surface production at the flame base (Fig. 3-CF, a). This instant corresponds to a positive pressure peak in the time trace in Fig. 4-CF , but the sound level of 70 dB (Tab. 1) remains moderate compared to the laboratory background noise 60 dB. Noise is mainly associated with phases of flame surface production.

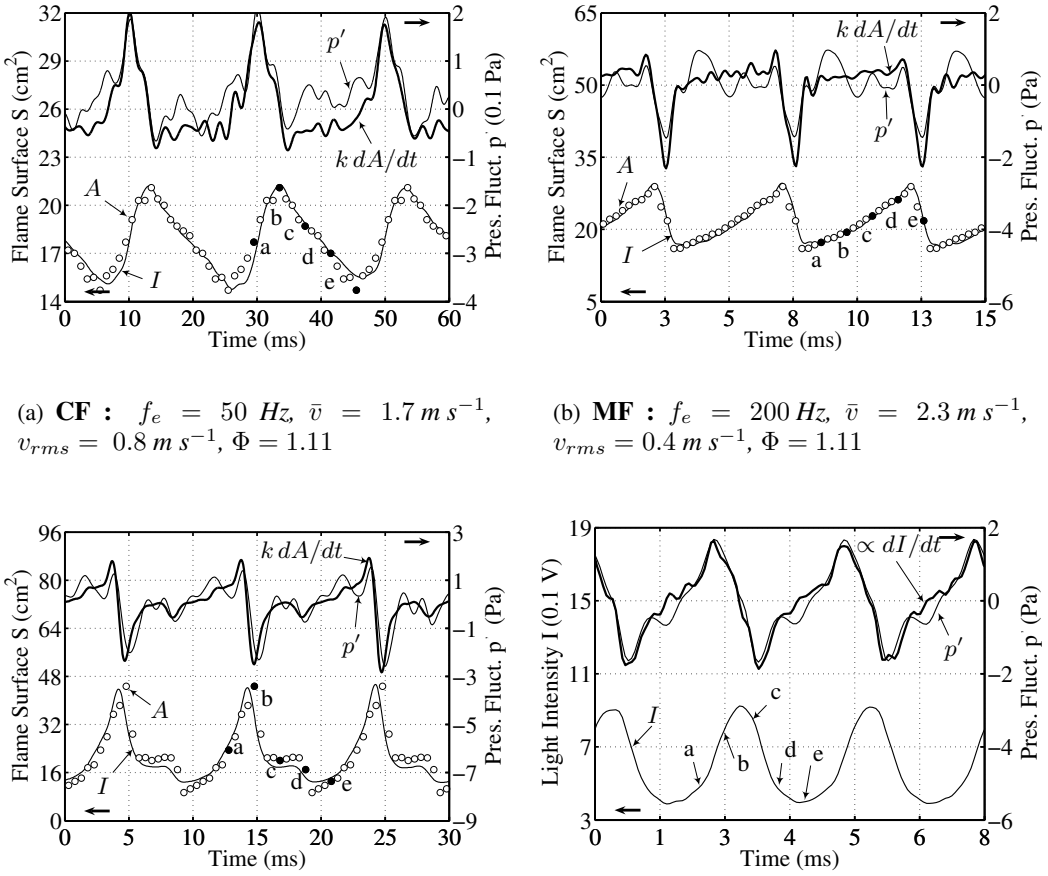

(a) **CF :** $f_e = 50\ Hz$, $\bar{v} = 1.7\ m\,s^{-1}$, $v_{rms} = 0.8\ m\,s^{-1}$, $\Phi = 1.11$

(b) **MF :** $f_e = 200\ Hz$, $\bar{v} = 2.3\ m\,s^{-1}$, $v_{rms} = 0.4\ m\,s^{-1}$, $\Phi = 1.11$

(c) **VF :** $f_e = 100\ Hz$, $\bar{v} = 2.3\ m\,s^{-1}$, $v_{rms} = 0.6\ m\,s^{-1}$, $\Phi = 1.11$

(d) **CSCF :** $f_e = 400\ Hz$, $\bar{v} = 5.0\ m\,s^{-1}$, $v_{rms} = 0.9\ m\,s^{-1}$, $\Phi = 0.95$

Figure 4: *Time traces : Rescaled OH* light intensity I, flame surface area A (circles), pressure fluctuations p' recorded by the microphone and pressure fluctuations computed from Eq. (4) :* $p' = k\,dA/dt$ *where* $k = \rho S_L\,(E-1)\,/4\pi r$. *Black circles marked* a, b, c, d *and* e *correspond to flames patterns presented in Fig. 3. Pressure signal* p' *has been shifted in time by* τ *to eliminate the acoustic propagation delay over the distance* r.

The sequence of images in Fig. 3-MF corresponds to an "M" shaped flame submitted to an harmonic forcing. It exhibits a different response than the conical flame. As the wrinkle travels towards the top of the flame, elements of neighboring fronts approach and pinch off (Fig. 3-MF, instants d and e). This mutual annihilation leads to the creation of a flame torus, which is convected downstream. The net result of this cyclic interaction is a flame surface variation $A_{rms}/\bar{A} = 0.19$ of the same order as the incoming flow perturbation level $v_{rms}/\bar{v} = 0.17$. The instant of flame pinching (Fig. 3-MF, e) corresponds to a large negative pressure peak (Fig. 4-MF), with an overall SPL equal to 90 dB (Tab. 1). In contrast to the previous case, noise is mainly associated to the fast rate of annihilation of the flame surface area. This in-

teraction results in a large sound level even for a relatively low flow modulation level. In the cycle presented in Fig. 3-VF, the rolling up motion at the flame periphery is due to a toroidal vortex shed from the burner lips generated by the flow perturbation at the burner outlet $v_{rms}/\bar{v} = 0.26$. This vortical structure is convected at half the mean flow velocity in the mixing layer formed at the premixed jet and the surrounding air interface towards the flame front [24]. As flame elements are rolled up at the front periphery, they are stretched, mutually interact (Fig. 3-VF, b-c) and contribute to a large rate of destruction of the flame surface area $A_{rms}/\bar{A} = 0.43$. This event corresponds to an intense negative pressure peak in Fig. 4-VF between instant b and c and results to a total SPL radiated of 94 dB. The last interaction explored involves an ensemble of small conical flames submitted to acoustic modulation that will be described in details below. Quantitative comparisons are now carried out.

Flame surface area A extracted from phase averaged images and indicated as circles in cm^2 are presented in Fig. 4 together with flame light intensity I displayed as solid lines. Emission signals I were rescaled using Eq. (6) to obtain quantities comparable to the flame surface area A. Both signals perfectly coincide during all phases of the driving cycle indicating that the flame dynamics can be well retrieved by examining OH^* radical light emission during flame interactions with a convective waves (Fig. 4-CF), mutual annihilation of flame elements (Fig. 4-MF) or flame vortex interactions (Fig. 4-VF). Time traces reveal strong non linearities during short phases of the driving cycles leading to either large rates of surface production (CF) or surface destruction (MF, VF). The radiated pressure p' measured by the microphone can be compared to the theoretical pressure fluctuation computed from the retarded rate of change of the flame surface area $k\,dA/dt$ using equation Eq. (4) where $k = \rho S_L\,(E-1)\,/4\pi r$. The signal dA/dt is derived from the rescaled light intensity I which is better temporally resolved than A. Results are plotted at the top of Figs. 4. Pressure peak positions, amplitudes and rms levels are correctly retrieved for the conical, "M" and "V" shaped flames submitted to convective waves (Figs. 4-CF, MF and VF). It should be noted that these results obtained for a microphone located in the near-field of the flame still obey the classical relation derived for far-field conditions.

The last interaction involving a collection of small conical flames differs to some extent from previous cases because phases of flame surface creation and destruction take approximatively the same duration (Fig. 4-CSCF). Instants of maximum rate of production and destruction correspond respectively to a positive and negative pressure peak of approximatively the same amplitude in pressure time trace in Fig. 4-CSCF. This observation differs from some of our previous expectations [11], that mechanisms leading to flame surface destruction were the main contributions to the overall noise production. Here, both creation and destruction phases result in opposite large rate of change of the flame surface area associated to intense pressure peaks. The flame surface area evolution was not extracted because flame contours are blurred in many images in Figs. 3-CSCF a-e due to the combined motion of each individual flame. Nevertheless, the flame dynamics can be described using flame emission signals. Letters in Fig. 4-CSCF indicate instants corresponding to images in Fig. 3-CSCF. The mean flow velocity at the plate holes outlet is $\bar{v} = 5.0$ m s^{-1} and the relative perturbation level $v_{rms}/\bar{v} = 0.16$ remains moderate. Flames first stretch and elongate quickly (Figs. 3-CSCF a and b) leading to large flame surface area production. Flames then suddenly break up and release small spher-

ical pockets of fresh reactions (Figs. 3-CSCF c and d). It is interesting to note that for about the same flow perturbation level $v_{rms} = 0.8 - 0.9$ m s^{-1}, the SPL radiated by the collection of small conical flames reaches 93 dB, whereas the single conical flame remains relatively quiet (CF, SPL = 70 dB, Tab. 1). It should also be mentioned that this result was obtained for a reduced mass flowrate $\dot{m} = 0.29$ g s^{-1} for the CSCF configuration to be compared with $\dot{m} = 0.59$ g s^{-1} consumed by the single conical flame (CF). The ensemble of small conical flames is a more compact configuration than the single conical flame leading to higher flame surface densities and to stronger noise production.

CONCLUSIONS

Flames perturbed by convective waves, vortex interactions, mutual annihilation of flame elements and collective effects define generic interactions and typify the more complex situation formed in most practical combusting systems. It is shown that these processes may induce large positive or negative rates of change of the heat release rate $d\dot{Q}/dt$ associated to respectively intense positive or negative pressure pulses. These mechanisms constitute intense sources of combustion noise which may dominate the overall radiated noise when they are organized and synchronized with coherent motions taking place inside the combustion chamber. It appears possible to reduce the noise level associated with combustion by minimizing the number and intensity of these events.

REFERENCES

References

[1] S. Candel, *Combustion dynamics and control : progress and challenges*, Proc. Comb. Inst., 29, (2002), 1–28.

[2] J. Mahan, A. Karchmer, *Combustion and core noise in Aeroacoustics of Flight Vehicles: Theory and Practice*, ed. H.H. Hubbard, NASA RP-1258, pp. 483–516 (1991).

[3] W. Strahle, *On combustion generated noise*, J. Fluid. Mech., 49, (1971), 399–414.

[4] H. Hassan, *Scaling of combustion-generated noise*, J. Fluid. Mech., 66, (1974), 445–453.

[5] S. Kotake, *On combustion noise related to chemical reactions*, J. Sound. Vib., 42, (1975), 399–410.

[6] W. Strahle, *Combustion noise*, Prog. Energy Combust. Sci., 4(3), (1978), 157–176.

[7] R. Doshiba, T. Hirano, *Mechanisms of sound generation from a premixed turbulent flame*, in *Sixteenth ICDERS*, Cracow (1997), pp. 432–435.

[8] R. Rajaram, T. Lieuwen, *Parametric studies of acoustic radiation from premixed flames*, Combust. Sci. and Tech., 175, (2003), 2269–2298.

[9] N. Kidin, V. Librovich, J. Roberts, M. Vuillermoz, *On sound sources in turbulent combustion*, AIAA Journal, 95, (1984), 343–355.

[10] J. M. Truffaut, *Etude expérimentale de l'origine du bruit émis par les flammes de chalumeaux*, Université de Provence (Aix-Marseille I), France (1998), ph. D. thesis.

[11] S. Candel, D. Durox, T. Schuller, *Flame interactions as a source of noise and combustion instabilities*, AIAA paper 2004-2928.

[12] G. Markstein, *Nonsteady flame propagation*, Marstein, G.H., Ed., Pergamon Press (1964).

[13] C. Law, *Dynamics of stretched flames*, in *Twenty-Second Symposium (International) on Combustion*, vol. 22, The Combustion Institute, Pittsburgh (1988), pp. 1381–1402.

[14] S. Bragg, *Combustion noise*, J. Inst. Fuel, 36, (1963), 12–16.

[15] P. Clavin, E. Siggia, *Turbulent premixed flames and sound generation*, Combust. Sci. Tech., 78, (1991), 147–155.

[16] I. Hurle, R. Price, T. Sugden, A. Thomas, *Sound emission from open turbulent flames*, Proc. R. Soc. A, 303, (1968), 409–427.

[17] R. B. Price, I. R. Hurle, T. M. Sudgen, *Optical studies of generation of noise in turbulent flames*, in *Twelfth Symposium (International) on Combustion*, The Combustion Institute, Pittsburgh (1969), pp. 1093–1102.

[18] B. N. Shivashankara, W. C. Strahle, J. C. Handley, *Evaluation of combustion noise scaling laws by an optical technique*, AIAA Journal, 13(5), (1975), 623–627.

[19] S. Kotake, K. Takamoto, *Combustion noise : Effects of the velocity turbulence of unburned mixture*, J. Sound. Vib., 139(1), (1990), 9–20.

[20] M. Katsuki, Y. Mizutani, M. Chikami, T. Kittaka, *Sound emission from a turbulent flame*, in *Twenty-first Symposium (International) on Combustion*, The Combustion Institute (1986), pp. 1543–1550.

[21] T. Schuller, D. Durox, S. Candel, *Dynamics of and noise radiated by a perturbed impinging premixed jet flame*, Combust. Flame, 128, (2002), 88–110.

[22] T. J. B. Smith, J. K. Kilham, *Noise generated by open turbulent flames*, J. Acoust. Soc. Am., 35(5), (1963), 715–724.

[23] C. Vagelopoulos, F. Egolfopoulos, C. Law, *Further considerations on the determination of laminar flame speeds with the counterflow twin-flame technique*, in *Twenty-Fifth Symposium (International) on Combustion*, vol. 25, The Combustion Institute, Pittsburgh (1994), pp. 1341–1347.

[24] D. Durox, T. Schuller, S. Candel, *Combustion dynamics of inverted conical flames*, Proc. Combust. Inst., 30(2), (2005), 1717–1724.